Transition-Metal-Promoted Reactions of Boron Hydrides. 16. Platinum- and Palladium-Catalyzed Olefin Addition and Olefin Dehydrogenative Borylation Reactions of *arachno*-6,8-$C_2B_7H_{13}$: Syntheses and Structural Characterizations of 7-R-*arachno*-6,8-$C_2B_7H_{12}$ and 7-(*trans*-R-CH═CH)-*arachno*-6,8-$C_2B_7H_{12}$

Daniel E. Kadlecek, Patrick J. Carroll, and Larry G. Sneddon*

Contribution from the Department of Chemistry, University of Pennsylvania, Philadelphia, Pennsylvania 19104-6323

Received June 19, 2000

Abstract: The chloroplatinic acid or platinum(II) bromide-catalyzed reaction of *arachno*-6,8-$C_2B_7H_{13}$ with ethylene results in hydroboration to yield the single product 7-(C_2H_5)-*arachno*-6,8-$C_2B_7H_{12}$. Analogous reactions with 1-pentene or styrene yield a mixture of both hydroboration, 7-R-*arachno*-6,8-$C_2B_7H_{12}$, and dehydrogenative borylation, 7-(*trans*-R-CH═CH)-*arachno*-6,8-$C_2B_7H_{12}$, products. On the other hand, the palladium(II) bromide-catalyzed reaction of *arachno*-6,8-$C_2B_7H_{13}$ with ethylene yields predominantly the dehydrogenative borylation product (7-(CH_2═CH)-*arachno*-6,8-$C_2B_7H_{12}$ along with smaller amounts of 7-(C_2H_5)-*arachno*-6,8-$C_2B_7H_{12}$. Palladium(II) bromide-catalyzed reactions with 1-pentene or styrene result in only dehydrogenative borylation to produce 7-(*trans*-R-CH═CH)-*arachno*-6,8-$C_2B_7H_{12}$. The hydroboration and dehydrogenative borylation products observed in the platinum- and palladium-catalyzed reactions are related to those that have been observed in recently reported metal-catalyzed hydrosilations and catecholborane or pinacolborane hydroborations and are consistent with a reaction mechanism involving competitive hydride-migration/reductive-elimination and boryl-migration/β-hydride-elimination steps. Crystallographic and DFT computational studies of the alkenyl-carbaboranes have also revealed unusual cage-bonding features that suggest π-bonding interactions of the B7 cage boron with its olefinic substituent.

Introduction

Because of the emerging uses[1] of organopolyboranes in such diverse applications as boron neutron capture agents, noncoordinating anions, extractants for radioactive wastes, and inorganic polymer components, the development of new systematic ways to functionalize polyboranes with organic substituents has been of great recent interest. We have previously shown that both platinum and palladium reagents can be used to catalyze the reactions of certain polyboranes with terminal olefins and thus provide selective, high-yield routes to their organo-substituted derivatives. For example, either chloroplatinic acid or platinum(II) bromide can be used to catalytically hydroborate terminal olefins with decaborane(14) to yield 6,9-$R_2B_{10}H_{12}$ derivatives in high yield.[2] Likewise, palladium(II) bromide catalyzes both olefin addition and olefin substitution reactions with pentaborane(9)[3,4] and borazine.[5] In this paper, we report that these metal reagents also catalyze the reactions of the *arachno*-6,8-$C_2B_7H_{13}$ dicarbaborane with terminal olefins to yield, depending upon the reaction conditions, metal reagent, and olefin, 7-alkyl- or 7-alkenyl-*arachno*-6,8-$C_2B_7H_{12}$ derivatives. We also report crystallographic and DFT computational studies of these products that reveal unusual cage-bonding features associated with the alkenyl substituents.

Experimental Section

All manipulations were carried out using standard high-vacuum or inert-atmosphere techniques as described by Shriver.[6]

Materials. Ethylene was obtained from MG Industries. Platinum(II) bromide, palladium(II) bromide, 1-pentene, and styrene were purchased from Aldrich and used as received. Chloroplatinic acid hexahydrate ($H_2PtCl_6 \cdot 6H_2O$) (38−40% Pt) was purchased from Strem. The *arachno*-6,8-$C_2B_7H_{13}$ was prepared according to literature methods.[7] Toluene was purchased from Fisher and distilled from sodium/benzophenone ketyl prior to use. Hexanes and Celite 545 were purchased from Fisher and used as received. Activated charcoal was purchased from J. T. Baker and used as received.

Physical Measurements. ^{1}H NMR spectra at 500.4 MHz, ^{11}B NMR spectra at 160.5 MHz, and ^{13}C NMR at 125.8 MHz were obtained on a Bruker AM-500 spectrometer equipped with the appropriate decoupling accessories. All ^{11}B chemical shifts are referenced to external $BF_3 \cdot O(C_2H_5)_2$ (0.00 ppm), with a negative sign indicating an upfield

(1) Plešek, J. *Chem. Rev.* **1992**, *92*, 269.
(2) Mazighi, K.; Carroll, P. J.; Sneddon, L. G. *Inorg. Chem.* **1993**, *32*, 1963.
(3) Davan, T.; Corcoran, E. W., Jr.; Sneddon, L. G. *Organometallics* **1983**, *2*, 1693.
(4) Corcoran, E. W., Jr.; Sneddon, L. G. In *Advances in Boron and the Boranes*; Liebman, J. F., Greenberg, A., Williams, R. E., Eds.; VCR: New York, 1988; p 71.
(5) Lynch, A. T.; Sneddon, L. G. *J. Am. Chem. Soc.* **1989**, *111*, 6201.
(6) Shriver, D. F.; Drezdzon, M. A. *Manipulation of Air-Sensitive Compounds*, 2nd ed.; Wiley: New York, 1986.
(7) Garrett, P. M.; George, T. A.; Hawthorne, M. F. *Inorg. Chem.* **1969**, *8*, 2008.

10.1021/ja002178r CCC: $19.00
Published on Web 10/21/2000

Table 1. Reaction Conditions and Product Ratios

olefin	catalyst[a]	substrate/olefin/ catalyst ratios	solvent	*T* (°C)	time (h)	conversion[c] (%)	alkyl/alkenyl ratio[c]	TON[d]	yield (alkyl/alkenyl) (%)[e]
ethylene	CPA	1.0/5.0/0.04	toluene	60	48	86	100/0	22	75/0
ethylene	$PtBr_2$	1.0/7.7/0.1	toluene	60	40	90	100/0	8	48/0
ethylene	$PdBr_2$	1.0/6.0/0.1	toluene	32	24	83	26/74	7	10/16
ethylene	$PdBr_2$	1.0/12.7/0.1	toluene	32	24	85	9/91	8	2/19
1-pentene	CPA	1.0/9.0/0.03	none[b]	60	20	88	43/57	27	5/14
1-pentene	$PtBr_2$	1.0/14.0/0.1	none[b]	22	90	89	38/62	9	31/25
1-pentene	$PdBr_2$	1.0/27.0/0.2	none[b]	32	6	84	0/100	4	0/53
styrene	CPA	1.5/10.0/0.1	toluene	60	35	74	34/66	12	41/48
styrene	$PtBr_2$	1.0/26.0/0.1	none[b]	22	24	86	43/57	8	43/21
styrene	$PdBr_2$	1.0/26.0/0.1	none[b]	32	18	85	0/100	8	0/49

[a] CPA = $H_2PtCl_6 \cdot 6H_2O$. [b] These reactions were run in neat olefin. [c] Determined by ^{11}B NMR. [d] Turnover number (TON) = moles of product divided by moles of catalyst, based on percent conversion by ^{11}B NMR. [e] Unoptimized isolated yields relative to the amount of starting material consumed.

Table 2. NMR Data

compound	nucleus	δ (multiplicity, intensity, assignment, *J* (Hz))
7-(C_2H_5)-*arachno*-6,8-$C_2B_7H_{12}$ (**1**)	^{11}B[a,b]	15.3 (s, B7), −1.4 (d, B5,9, J_{BH} 153), −18.3 (d, B2,3, J_{BH} 161), −30.9 (d, B4, J_{BH} 141), −50.2 (d, B1, J_{BH} 152)
	^{11}B(calcd)[c,d]	16.6 (B7), −2.1 (B5,9), −16.0 (B2,3), −31.5 (B4), −53.8 (B1)
	$^{11}B-^{11}B$[a,e]	observed cross-peaks: B1−B2,3; B1−B4; B1−B5,9; B2,3−B5,9; B2,3−B7
	$^{1}H\{^{11}B\}$[a,f]	3.23 (2, BH), 2.32 (2, BH), 2.00 (1, BH), 1.07 (m, 2, CH_2CH_3), 1.03 (m, 3, CH_2CH_3), 0.44 (1, BH), −0.39 (s, 2, cage-CH), −2.06 (s, 2, cage-CH), −2.65 (2, BHB)
	$^{13}C\{^{1}H\}$[a,g]	12.65 (C11), 10.45 (C10, $J_{^{13}C-^{11}B}$ 72), −11.57 (C6,8)
	^{13}C(calcd)[c,d]	15.48 (C10), 13.18 (C11), −9.09 (C6,8)
7-(CH_2=CH)-*arachno*-6,8-$C_2B_7H_{12}$ (**2**)	^{11}B[a,b]	9.0 (s, B7), −1.3 (d, B5,9, J_{BH} 153), −17.1 (d, B2,3, J_{BH} 162), −29.8 (d, B4, J_{BH} 161), −49.9 (d, B1, J_{BH} 149)
	^{11}B(calcd)[c,d]	10.9 (B7), −2.4 (B5,9), −14.9 (B2,3), −30.8 (B4), −53.1 (B1)
	$^{1}H\{^{11}B\}$[a,f]	6.46 (dd, 1, C*H*=CH_2, $^3J_{HH}$ 18, $^3J_{HH}$ 13), 5.76 (d, 1, CH=CH_2, $^3J_{HH}$ 13), 5.59 (d, 1, CH=CH_2, $^3J_{HH}$ 18), 3.31 (2, BH), 2.55 (2, BH), 2.10 (1, BH), 0.60 (1, BH), −0.06 (s, 2, cage-CH), −1.71 (s, 2, cage-CH), −2.49 (2, BHB)
	$^{13}C\{^{1}H\}$[g,h]	126.71, −11.32 (C6,8)
	^{13}C(calcd)[c,d]	146.38 (C10), 129.72 (C11), −9.92 (C6,8)
7-($CH_3(CH_2)_2$CH=CH)-*arachno*-6,8-$C_2B_7H_{12}$ (**3**)	^{11}B[a,b]	10.3 (s, B7), −1.8 (d, B5,9, J_{BH} 146), −17.7 (d, B2,3, J_{BH} 161), −30.5 (d, B4, J_{BH} 128), −49.5 (d, B1, J_{BH} 148)
	$^{1}H\{^{11}B\}$[a,f]	5.91 (m, 2, vinyl), 3.20 (2, BH), 2.44 (2, BH), 2.11 (m, 2, CH), 1.95 (1, BH), 1.43 (m, 2, CH), 0.93 (m, 3, CH), 0.54 (1, BH), −0.15 (s, 2, cage-CH), −1.82 (s, 2, cage-CH), −2.59 (2, BHB)
	$^{13}C\{^{1}H\}$[g,i]	143.58, 128.48 ($J_{^{13}C-^{11}B}$ 108), 37.75, 22.13, 13.73, −11.29 (C6,8)
7-(C_5H_{11})-*arachno*-6,8-$C_2B_7H_{12}$ (**4**)	^{11}B[a,b]	14.8 (s, B7), −1.4 (d, B5,9, J_{BH} 154), −18.2 (d, B2,3, J_{BH} 162), −30.8 (d, B4, J_{BH} 153), −50.2 (d, B1, J_{BH} 147)
	$^{1}H\{^{11}B\}$[a,f]	3.23 (2, BH), 2.32 (2, BH), 2.05 (1, BH), 1.38 (m, 6, CH), 1.10 (m, 2, CH), 0.98 (m, 3, CH), 0.50 (1, BH), −0.35 (s, 2, cage-CH), −1.99 (s, 2, cage-CH), −2.63 (2, BHB)
7-((C_6H_5)CH=CH)-*arachno*-6,8-$C_2B_7H_{12}$ (**5**)	^{11}B[a,b]	9.6 (s, B7), −1.4 (d, B5,9, J_{BH} 144), −17.1 (d, B2,3, J_{BH} 157), −29.9 (d, B4, J_{BH} 145), −49.6 (d, B1, J_{BH} 150)
	$^{1}H\{^{11}B\}$[a,f]	7.37−7.04 (m, 5, phenyl), 6.92−6.78 (dd, 2, vinyl), 3.36 (2, BH), 2.64 (2, BH), 2.13 (1, BH), 0.68 (1, BH), 0.05 (s, 2, cage-CH), −1.60 (s, 2, cage-CH), −2.41 (2, BHB)
7-((C_6H_5)CH_2CH_2)-*arachno*-6,8-$C_2B_7H_{12}$ (**6**)	^{11}B[a,b]	13.7 (s, B7), −1.1 (d, B5,9, J_{BH} 152), −17.9 (d, B2,3, J_{BH} 159), −30.5 (d, B4),[j] −50.4 (d, B1, J_{BH} 149)
	$^{1}H\{^{11}B\}$[a,f]	7.36−7.23 (m, 5, phenyl), 3.34 (2, BH), 2.77 (m, 2, CH), 2.46 (2, BH), 2.11 (1, BH), 1.56 (m, 2, CH), 0.56 (1, BH), −0.29 (m, 2, cage-CH), −1.87 (m, 2, cage-CH), −2.54 (2, BHB)

[a] C_6D_6. [b] 160.5 MHz. [c] B3LYP/6-311G*//B3LYP/6-311G*. [d] Although the calculated static structures have C_1 symmetry, free rotation of the alkyl/alkenyl substituent in solution would generate C_s symmetric structures and B2/B3, B5/B9, and C6/C8 would become equivalent. Thus, the calculated chemical shift values for these atoms in this table are the average of the calculated static values (ppm): (**1**) B2 (−15.0), B3 (−16.9); B5 (−2.1), B9 (−2.2); C6 (−7.65), C8 (−10.52); (**2**) B2 (−15.9), B3 (−13.9); B5 (−3.1), B9 (−1.7); C6 (−6.88), C8 (−12.96). [e] 64.2 MHz. [f] 500.4 MHz. [g] 125.8 MHz. [h] CD_2Cl_2. [i] $CDCl_3$. [j] J_{BH} not resolved.

shift. All ^1H and ^{13}C chemical shifts were measured relative to internal residual protons or carbons in the lock solvent and are referenced to Me_4Si (0.00 ppm). Gas chromatography/mass spectrometry (GC/MS) was performed on a Hewlett-Packard 5890A gas chromatograph (equipped with a cross-linked methylsilicone column) interfaced to a Hewlett-Packard 5970 mass selective detector. Infrared spectra were obtained on a Perkin-Elmer 1430 spectrophotometer. Flash column chromatography was performed using silica gel (230−400 mesh, Merck). Elemental analyses were performed at the University of Pennsylvania microanalysis facility. Melting points were obtained on a standard melting point apparatus and are uncorrected.

$H_2PtCl_6 \cdot 6H_2O$- and $PtBr_2$-Catalyzed Reactions of Ethylene. As given in Table 1, the *arachno*-6,8-$C_2B_7H_{13}$ and either $H_2PtCl_6 \cdot 6H_2O$ or $PtBr_2$ were charged into an 88 mL Andrews Glass pressure reaction vessel (part no. 110-207-0003) equipped with a Whitey needle valve and a magnetic stirbar. Toluene (10 mL) and ethylene (measured by expansion of the gas into a known volume) were vacuum transferred into the vessel, and then the mixtures were immersed and stirred in an

oil bath. Following termination of the reaction, isolation and purification of the products by filtering the product mixture through a 1/1 mixture of Celite 545/activated charcoal followed by flash column chromatography (hexanes) yielded pure 7-(C_2H_5)-*arachno*-6,8-$C_2B_7H_{12}$ (**1**) (Table 1): white solid; $R_f = 0.18$; mp 40.5−41.5 °C; IR (NaCl, cm^{-1}) 3060 (w), 3000 (w), 2950 (m), 2800 (w), 2760 (w), 2580 (vs), 2010 (w), 1450 (w), 1410 (w), 1380 (w), 1290 (w), 1160 (m), 1080 (m), 1060 (m), 1030 (m), 980 (w), 890 (m), 840 (w), 670 (w). Anal. Calcd: C, 34.11; H, 12.17. Found: C, 34.56; H, 12.42.

$PtBr_2$-catalyzed reactions run at room temperature resulted in very low conversions to a mixture of products corresponding to **1** and 7-(CH_2═CH)-*arachno*-6,8-$C_2B_7H_{12}$ (**2**) (vide infra).

$PdBr_2$-Catalyzed Reaction of Ethylene. As outlined in Table 1, *arachno*-6,8-$C_2B_7H_{13}$ and $PdBr_2$ were reacted in toluene solution according to the procedures described above. Isolation and purification of the products by filtering the product mixture through a 1/1 Celite 545/activated charcoal plug followed by flash column chromatography (2/1 hexanes/toluene) yielded pure 7-(C_2H_5)-*arachno*-6,8-$C_2B_7H_{12}$ (**1**) ($R_f = 0.56$) and 7-(CH_2═CH)-*arachno*-6,8-$C_2B_7H_{12}$ (**2**) ($R_f = 0.48$) (Table 1). Data for **2**: clear solid; mp < room temperature; IR (NaCl, cm^{-1}) 3075 (m), 2970 (s), 2930 (m), 2590 (vs), 2340 (m), 2320 (m), 1620 (m), 1545 (m), 1460 (w), 1420 (w), 1380 (m), 1260 (s), 1090 (m), 1060 (m), 1040 (m), 1010 (m), 890 (m). HRMS (*m*/*e*) calcd for $^{12}C_4{}^{11}B_7{}^1H_{14}$ (M − H) 139.1747, found 139.1784.

$H_2PtCl_6·6H_2O$- and $PtBr_2$-Catalyzed Reactions of 1-Pentene and Styrene. As given in Table 1, the *arachno*-6,8-$C_2B_7H_{13}$ and either $H_2PtCl_6·6H_2O$ or $PtBr_2$ were added to a 100 mL Schlenk tube, equipped with a magnetic stirbar, under a N_2 purge. Either 1-pentene or styrene was added via syringe, and then the reaction vessel was degassed on the high-vacuum line. The chloroplatinic acid-catalyzed reactions were stirred in a 60 °C oil bath, while the $PtBr_2$-catalyzed reactions were stirred at room temperature. In the chloroplatinic acid-catalyzed reaction with styrene, toluene (3 mL) was added to prevent gelling of the solution.

The reaction products were isolated and purified by passing the product mixture through a 1/1 mixture of Celite 545/activated charcoal followed by flash column chromatography to yield analytically pure samples (Table 1). For 1-pentene: 7-(*trans*-$CH_3(CH_2)_2CH$═CH)-*arachno*-6,8-$C_2B_7H_{12}$ (**3**) and 7-(C_5H_{11})-*arachno*-6,8-$C_2B_7H_{12}$ (**4**). Data for **3**: white solid; R_f(hexanes) = 0.13; mp 48.5−49.5 °C; IR (NaCl, cm^{-1}) 3060 (w), 2980 (w), 2940 (m), 2920 (m), 2860 (w), 2560 (vs), 2000 (w), 1620 (s), 1450 (w), 1420 (w), 1370 (w), 1170 (m), 1080 (m), 1060 (m), 1020 (w), 970 (m), 890 (m), 660 (w). Anal. Calcd: C, 46.47; H, 11.70. Found: C, 46.67; H, 11.84. Data for **4**: pale yellow oil; R_f(hexanes) = 0.21; IR (NaCl, cm^{-1}) 3050 (m), 3000 (m), 2940 (s), 2910 (s), 2860 (m), 2840 (m), 2560 (vs), 2010 (w), 1710 (w), 1630 (w), 1470 (m), 1460 (m), 1410 (w), 1370 (w), 1220 (w), 1180 (w), 1160 (m), 1080 (m), 1060 (m), 1030 (m), 1020 (m), 980 (s), 890 (s), 680 (m). Anal. Calcd: C, 45.96; H, 12.67. Found: C, 46.60; H, 11.84. For styrene: 7-(*trans*-(C_6H_5)CH═CH)-*arachno*-6,8-$C_2B_7H_{12}$ (**5**) and 7-((C_6H_5)CH_2CH_2)-*arachno*-6,8-$C_2B_7H_{12}$ (**6**). Data for **5**: white solid; R_f(2/1 hexanes/toluene) = 0.35; mp 101.0−102.5 °C; IR (NaCl, cm^{-1}) 3060 (w), 3020 (w), 2990 (w), 2920 (w), 2560 (s), 1600 (m), 1480 (s), 1440 (s), 1410 (s), 1390 (s), 1380 (s), 1290 (w), 1250 (w), 1190 (m), 1180 (m), 1080 (w), 1060 (m), 1020 (m), 980 (w), 890 (m), 690 (m), 670 (m); HRMS (*m*/*e*) calcd for $^{12}C_{10}{}^{11}B_7{}^1H_{19}$ 216.2138, found 216.2146. Data for **6**: white solid; R_f(2/1 hexanes/toluene) = 0.51; mp 61.5−62.5 °C; IR (NaCl, cm^{-1}) 3040 (w), 3000 (w), 2980 (w), 2930 (w), 2910 (w), 2560 (s), 2500 (m), 1480 (w), 1440 (w), 1400 (w), 1370 (w), 1250 (m), 1150 (w), 1080 (m), 1060 (m), 1020 (m), 990 (w), 890 (m), 690 (w), 660 (w); HRMS (*m*/*e*) calcd for $^{12}C_{10}{}^{11}B_7{}^1H_{20}$ (M − H) 217.2216, found 217.2225.

$PdBr_2$-Catalyzed Reactions of 1-Pentene and Styrene. As given in Table 1, the *arachno*-6,8-$C_2B_7H_{13}$ and $PdBr_2$ were added to a N_2-flushed 100 mL Schlenk tube equipped with a magnetic stirbar. The 1-pentene or styrene was added via syringe through the neck of the reaction vessel, and then the mixture was degassed on the high-vacuum line. The mixture was immersed in an oil bath with stirring. Flash column chromatography (2/1 hexanes/toluene) of the 1-pentene and styrene product mixtures with subsequent concentration of appropriate fractions resulted in the isolation of analytically pure samples of 7-(*trans*-$CH_3(CH_2)_2CH$═CH)-*arachno*-6,8-$C_2B_7H_{12}$ (**3**) ($R_f = 0.61$) and 7-(*trans*-(C_6H_5)CH═CH)-*arachno*-6,8-$C_2B_7H_{12}$ (**5**), respectively (Table 1).

Crystallographic Data for Compounds 1, 3, and 5. Colorless crystals of 7-(C_2H_5)-*arachno*-6,8-$C_2B_7H_{12}$ (**1**) were grown by slow evaporation of a hexanes solution at −25 °C in a drybox. Colorless crystals of 7-(*trans*-$CH_3(CH_2)_2CH$═CH)-*arachno*-6,8-$C_2B_7H_{12}$ (**3**) were grown by sublimation in a sealed NMR tube placed 3 in. above a hot plate held at 60 °C. Colorless crystals of 7-(*trans*-(C_6H_5)CH═CH)-*arachno*-6,8-$C_2B_7H_{12}$ (**5**) were grown by slow evaporation of a CH_2Cl_2/hexanes solution at −25 °C in a drybox.

Collection and Reduction of the Data. X-ray intensity data were collected on a Rigaku R-AXIS IIc area detector employing graphite-monochromated Mo Kα radiation ($\lambda = 0.710\,69$ Å) at a temperature of 198 K. Indexing was performed from a series of 1° oscillation images with exposures of 15 min/frame. A hemisphere of data was collected using 10° oscillation angles with exposures of 20 min/frame and a crystal-to-detector distance of 82 mm. Oscillation images were processed using bioteX,[8] producing a listing of unaveraged F^2 and $\sigma(F^2)$ values which were then passed to the teXsan[9] program package for further processing and structure solution on a Silicon Graphics Indigo R4000 computer. The intensity data were corrected for Lorentz and polarization effects but not for absorption.

Solution and Refinement of the Structures. The structures were solved by direct methods (SIR92).[10] Refinement was by full-matrix least-squares based on F^2 using SHELXL-93.[11] All reflections were used during refinement (F^2 values that were experimentally negative were replaced by $F^2 = 0$). The weighting scheme used was $w = 1/[\sigma^2(F_o^2) + 0.0321P^2 + 0.4162P]$, where $P = (F_o^2 + 2F_c^2)/3$. Non-hydrogen atoms were refined anisotropically, and hydrogen atoms were refined isotropically. Crystal and refinement data are given in Table 3. Refined positional parameters are given in the Supporting Information. Selected intramolecular bond distances and angles are given in Tables 4 and 5.

Computational Studies. The DFT/GIAO/NMR method,[12] using the Gaussian 94 program,[13] was used in a manner similar to that previously described.[14−16] The geometries were fully optimized at the B3LYP/6-311G* level within the specified symmetry constraints (using the standard basis sets included) on a (2)-processor Origin 2000 computer running IRIX 6.5.5 or a (6)-processor Power Challenge XL computer running IRIX 6.5.6. A vibrational frequency analysis was carried out on each optimized geometry at the B3LYP/6-311G* level with a true minimum found for each structure (i.e., possessing no imaginary frequencies). The NMR chemical shifts were calculated at the B3LYP/6-311G* level using the GIAO option within Gaussian 94. ^{11}B NMR GIAO chemical shifts are referenced to $BF_3·O(C_2H_5)_2$ using an absolute shielding constant of 102.24.[15,17] The ^{13}C NMR GIAO chemical shifts

(8) bioteX: A suite of programs for the Collection, Reduction and Interpretation of Imaging Plate Data, Molecular Structure Corp., 1995.

(9) teXsan: Crystal Structure Analysis Program, Molecular Structure Corp., 1985, 1992.

(10) SIR92: Altomare, A.; Burla, M. C.; Camalli, M.; Cascarano, M.; Giacovazzo, C.; Guagliardi, A.; Polidoro, G. *J. Appl. Crystallogr.* **1994**, *27*, 435.

(11) SHELXL-93: Program for the Refinement of Crystal Structures, G. M. Sheldrick, University of Göttingen, Germany, 1993.

(12) Yang, X.; Jiao, H.; Schleyer, P. v. R. *Inorg. Chem.* **1997**, *36*, 4897 and references therein.

(13) *Gaussian 94*, Revision E.2: Frisch, M. J.; Trucks, G. W.; Schlegel, H. B.; Gill, P. M. W.; Johnson, B. G.; Robb, M. A.; Cheeseman, J. R.; Keith, T.; Peterson, G. A.; Montgomery, J. A.; Raghavachari, K.; Al-Laham, M. A.; Zakrzewski, V. G.; Ortiz, J. V.; Foresman, J. B.; Cioslowski, J.; Stefanov, B. B.; Nanayakkara, A.; Challacombe, M.; Peng, C. Y.; Ayala, P. T.; Chen, W.; Wong, M. W.; Andres, J. L.; Replogle, E. S.; Gomperts, R.; Martin, R. L.; Fox, D. J.; Binkley, J. S.; Defrees, D. J.; Baker, J.; Stewart, J. P.; Head-Gordon, M.; Gonzalez, C.; Pople, J. A. Gaussian, Inc., Pittsburgh, PA, 1995.

(14) Keller, W.; Barnum, B. A.; Bausch, J. W.; Sneddon, L. G. *Inorg. Chem.* **1993**, *32*, 5058.

(15) Bausch, J. W.; Rizzo, R. C.; Sneddon, L. G.; Wille, A. E.; Williams, R. E. *Inorg. Chem.* **1996**, *35*, 131.

(16) Tebben, A. J. M.S. Thesis, Villanova University, 1997.

(17) Tebben, A. J.; Bausch, J. W. Private communication.

Table 3. Crystallographic Data Collection and Structure Refinement Information

	1	**3**	**5**
empirical formula	$C_4B_7H_{17}$	$C_7B_7H_{21}$	$C_{10}B_7H_{19}$
formula weight	140.85	180.91	214.92
crystal class	monoclinic	monoclinic	monoclinic
space group	$P2_1/c$ (no. 14)	$C2/c$ (no. 15)	$P2_1/n$ (no. 14)
Z	4	8	4
cell constants			
a (Å)	13.8757(11)	20.8838(4)	11.4347(4)
b (Å)	6.8831(6)	5.5168(2)	12.0143(5)
c (Å)	10.1842(10)	20.8943(8)	10.5920(3)
β (deg))	101.813(4)	90.056(2)	114.156(2)
V (Å^3)	952.1(2)	2407.27(14)	1327.71(8)
μ (cm^{-1})	0.43	0.46	0.52
crystal size (mm)	0.35 × 0.12 × 0.04	0.38 × 0.22 × 0.04	0.48 × 0.40 × 0.36
D_{calcd} (g/cm^3)	0.983	0.998	1.075
F(000)	304	784	456
radiation	Mo Kα (λ = 0.710 69 Å)	Mo Kα (λ = 0.710 69 Å)	Mo Kα (λ = 0.710 69 Å)
2θ range (deg)	6.00−50.68	5.52−50.7	5.18−50.74
hkl collected	$-16 \le h \le \pm 16$	$-24 \le h \le \pm 24$	$-13 \le h \le \pm 13$
	$-8 \le k \le \pm 8$	$-6 \le k \le \pm 6$	$-14 \le k \le \pm 14$
	$-12 \le l \le \pm 11$	$-25 \le l \le \pm 25$	$-12 \le l \le \pm 12$
no. of reflns measd	5251	8846	9941
no. of unique reflns	1697 (R_{int} = 0.0456)	2064 (R_{int} = 0.0422)	2398 (R_{int} = 0.0332)
no. of obsd reflns	1456 ($F > 4\sigma$)	1880 ($F > 4\sigma$)	2182 ($F > 4\sigma$)
no. of reflns used in refinement	1697	2064	2398
no. of params	169	211	231
R[a] indices ($F > 4\sigma$)	R1 = 0.0775	R1 = 0.0532	R1 = 0.0537
	wR2 = 0.1362	wR2 = 0.1132	wR2 = 0.1168
R[a] indices (all data)	R1 = 0.0927	R1 = 0.0603	R1 = 0.0605
	wR2 = 0.1416	wR2 = 0.1165	wR2 = 0.1205
GOF	1.297	1.149	1.154
final difference peaks (e/Å^3)	+0.131, 0.115	+0.120, 0.099	+0.141, 0.127

[a] $R1 = \sum||F_o| - |F_c||/\sum|F_o|$; $wR2 = \{\sum w(F_o^2 - F_c^2)^2/\sum w(F_o^2)^2\}^{1/2}$.

Table 4. Comparison of Selected Crystallographically Determined and DFT-Calculated (B3LYP/6-311G* Level) Bond Lengths (Å) and Angles (deg) for **1**

	X-ray Bond Lengths		
B(7)−C(10)	1.562(3)	B(2)−B(7)	1.742(4)
C(10)−C(11)	1.520(4)	B(3)−B(7)	1.740(3)
B(7)−C(6)	1.723(3)	B(5)−C(6)	1.682(3)
B(7)−C(8)	1.736(4)	B(9)−C(8)	1.671(3)
B(2)−C(6)	1.667(3)	B(3)−C(8)	1.663(3)
	X-ray Bond Angles		
C(11)−C(10)−B(7)	115.4(2)	C(6)−B(7)−C(8)	106.8(2)
C(10)−B(7)−C(6)	120.8(2)	B(5)−C(6)−B(7)	114.5(2)
C(10)−B(7)−C(8)	122.2(2)	B(9)−C(8)−B(7)	114.4(2)
C(10)−B(7)−B(2)	128.1(2)	C(8)−B(7)−B(3)	57.2(1)
C(10)−B(7)−B(3)	128.8(2)	C(6)−B(7)−B(2)	57.5(1)
	DFT Bond Lengths		
B(7)−C(10)	1.583	B(2)−B(7)	1.743
C(10)−C(11)	1.537	B(3)−B(7)	1.741
B(7)−C(6)	1.738	B(5)−C(6)	1.695
B(7)−C(8)	1.742	B(9)−C(8)	1.691
B(2)−C(6)	1.679	B(3)−C(8)	1.678
	DFT Bond Angles		
C(11)−C(10)−B(7)	116.2	C(6)−B(7)−C(8)	106.2
C(10)−B(7)−C(6)	120.2	B(5)−C(6)−B(7)	113.9
C(10)−B(7)−C(8)	122.3	B(9)−C(8)−B(7)	113.8
C(10)−B(7)−B(2)	128.3	C(8)−B(7)−B(3)	57.6
C(10)−B(7)−B(3)	129.7	C(6)−B(7)−B(2)	57.7

are referenced to TMS using an absolute shielding constant of 184.38 and are corrected according to the method described by Schleyer.[18]

Results

Chloroplatinic Acid- and Platinum(II) Bromide-Catalyzed Reaction of Ethylene with *arachno*-6,8-$C_2B_7H_{13}$. The reaction of ethylene with *arachno*-6,8-$C_2B_7H_{13}$ in toluene solution at 60 °C in the presence of either $H_2PtCl_6{\cdot}6H_2O$ (4.0 mol %, 48 h) or $PtBr_2$ (10.0 mol %, 40 h) (Table 1) resulted in ethylene hydroboration to produce 7-(C_2H_5)-*arachno*-6,8-$C_2B_7H_{12}$ (**1**) (eq 1) as the sole product.

$$\textit{arachno}\text{-}6,8\text{-}C_2B_7H_{13} + \text{xs } H_2C{=}CH_2 \xrightarrow[60\ ^\circ C,\ PhCH_3]{H_2PtCl_6{\cdot}6H_2O \text{ or } PtBr_2} \underset{\mathbf{1}}{7\text{-}(C_2H_5)\text{-}\textit{arachno}\text{-}6,8\text{-}C_2B_7H_{12}} \quad (1)$$

GC/MS and ^{11}B NMR analyses of the product mixtures resulting from the $H_2PtCl_6{\cdot}6H_2O$- and $PtBr_2$-catalyzed reactions indicated 86% and 90% conversions, respectively, corresponding to 22 and 8 turnovers for the two catalysts. Filtration of the reaction mixtures and removal of the volatiles under reduced pressure resulted in the isolation of an oily material that was shown by GC/MS to be the single product **1**, contaminated with trace amounts of unreacted *arachno*-6,8-$C_2B_7H_{13}$. Further purification by flash column chromatography to remove the unreacted *arachno*-6,8-$C_2B_7H_{13}$ afforded analytically pure samples of crystalline 7-(C_2H_5)-*arachno*-6,8-$C_2B_7H_{12}$ (**1**) in 75% and 48% isolated yields for the $H_2PtCl_6{\cdot}6H_2O$- and $PtBr_2$-catalyzed reactions, respectively.

Longer reaction times and higher temperatures resulted in the production of more highly substituted products that could not be easily separated by chromatographic methods. Lowering the temperature of the chloroplatinic acid-catalyzed reactions resulted in no reaction. Likewise, decreasing the temperature of the platinum(II) bromide-catalyzed reaction decreased the rate (~5% conversion in 20 h), but also yielded a product mixture that contained both **1** and small amounts of the dehydrogenative borylation product 7-($CH_2{=}CH$)-*arachno*-6,8-$C_2B_7H_{12}$ (**2**).

(18) Maerker, C.; Schleyer, P. v. R.; Salahub, D. R.; Malkina, O. L.; Malkin, V. G. Private communication.

Table 5. DFT-Calculated (B3LYP/6-311G* Level) Bond Lengths (Å) and Angles (deg) for **2** and Crystallographically Determined Bond Lengths (Å) and Angles (deg) for **3** and **5**

	Bond Lengths for **2**		
B(7)−C(10)	1.555	B(2)−B(7)	1.744
C(10)−C(11)	1.336	B(3)−B(7)	1.749
B(7)−C(6)	1.747	B(5)−C(6)	1.691
B(7)−C(8)	1.715	B(9)−C(8)	1.711
B(2)−C(6)	1.676	B(3)−C(8)	1.683
	Bond Angles for **2**		
C(11)−C(10)−B(7)	126.4	C(6)−B(7)−C(8)	107.0
C(10)−B(7)−C(6)	119.7	B(5)−C(6)−B(7)	113.7
C(10)−B(7)−C(8)	123.4	B(9)−C(8)−B(7)	113.5
C(10)−B(7)−B(2)	126.0	C(8)−B(7)−B(3)	58.1
C(10)−B(7)−B(3)	128.9	C(6)−B(7)−B(2)	57.4
	Bond Lengths for **3**		
B(7)−C(10)	1.546(2)	B(2)−B(7)	1.745(3)
C(10)−C(11)	1.322(2)	B(3)−B(7)	1.752(2)
B(7)−C(6)	1.741(2)	B(5)−C(6)	1.669(2)
B(7)−C(8)	1.713(2)	B(9)−C(8)	1.689(2)
B(2)−C(6)	1.663(2)	B(3)−C(8)	1.669(2)
	Bond Angles for **3**		
C(11)−C(10)−B(7)	126.5(2)	C(6)−B(7)−C(8)	107.8(1)
C(10)−B(7)−C(6)	119.9(1)	B(5)−C(6)−B(7)	114.6(1)
C(10)−B(7)−C(8)	122.2(1)	B(9)−C(8)−B(7)	114.4(1)
C(10)−B(7)−B(2)	127.5(1)	C(8)−B(7)−B(3)	57.5(1)
C(10)−B(7)−B(3)	129.6(1)	C(6)−B(7)−B(2)	57.0(1)
	Bond Lengths for **5**		
B(7)−C(10)	1.548(2)	B(2)−B(7)	1.745(3)
C(10)−C(11)	1.335(2)	B(3)−B(7)	1.752(3)
B(7)−C(6)	1.722(2)	B(5)−C(6)	1.679(3)
B(7)−C(8)	1.709(2)	B(9)−C(8)	1.695(2)
B(2)−C(6)	1.663(3)	B(3)−C(8)	1.667(2)
	Bond Angles for **5**		
C(11)−C(10)−B(7)	126.5(2)	C(6)−B(7)−C(8)	107.2(1)
C(10)−B(7)−C(6)	119.9(1)	B(5)−C(6)−B(7)	114.1(1)
C(10)−B(7)−C(8)	123.4(1)	B(9)−C(8)−B(7)	114.5(1)
C(10)−B(7)−B(2)	126.3(1)	C(8)−B(7)−B(3)	57.6(1)
C(10)−B(7)−B(3)	128.7(1)	C(6)−B(7)−B(2)	57.4(1)

Palladium(II) bromide-Catalyzed Reaction of Ethylene with *arachno*-6,8-$C_2B_7H_{13}$. In contrast to the platinum-catalyzed reactions, the $PdBr_2$ (10 mol %, 24 h) catalyzed reaction of ethylene with *arachno*-6,8-$C_2B_7H_{13}$ in toluene (Table 1) resulted in mainly dehydrogenative borylation to produce **2** (74%) as the major product, with the hydroboration product **1** (26%) being produced in much smaller amounts (eq 2). Minor amounts of higher substituted products and unreacted *arachno*-6,8-$C_2B_7H_{13}$ were also present in the product mixture.

$$\textit{arachno}\text{-}6,8\text{-}C_2B_7H_{13} + \text{xs } H_2C{=}CH_2 \xrightarrow[32\ ^\circ C,\ PhCH_3]{PdBr_2} \underset{\mathbf{1}}{7\text{-}(C_2H_5)\text{-}\textit{arachno}\text{-}6,8\text{-}C_2B_7H_{12}} + \underset{\mathbf{2}}{7\text{-}(CH_2{=}CH)\text{-}\textit{arachno}\text{-}6,8\text{-}C_2B_7H_{12}} \quad (2)$$

The **1**/**2** product ratio was found to be dependent on the ethylene concentration, with an increase in the ethylene concentration (Table 1) favoring the formation of **2** (91%) relative to **1** (9%). Although the conversion rates and product yields were high according to NMR analysis, the isolated yields (Table 1) of pure materials were greatly reduced owing to decomposition during the chromatographic separation.

Chloroplatinic Acid and Platinum(II) Bromide-Catalyzed Reactions of 1-Pentene and Styrene with *arachno*-6,8-$C_2B_7H_{13}$. The platinum-catalyzed reactions of ethylene with *arachno*-6,8-$C_2B_7H_{13}$ gave exclusively the hydroboration product, while the $H_2PtCl_6{\cdot}6H_2O$- or $PtBr_2$-catalyzed reaction with 1-pentene or styrene (Table 1) resulted in both hydroboration and dehydrogenative borylation to yield a mixture of the 7-alkyl- and 7-alkenyl-*arachno*-6,8-$C_2B_7H_{12}$ derivatives as given in eqs 3 and 4.

$$\textit{arachno}\text{-}6,8\text{-}C_2B_7H_{13} + \text{xs } H_2C{=}CH(CH_2)_2CH_3 \xrightarrow{H_2PtCl_6{\cdot}6H_2O \text{ or } PtBr_2} \underset{\mathbf{3}}{7\text{-}(\textit{trans}\text{-}CH_3(CH_2)_2CH{=}CH)\text{-}\textit{arachno}\text{-}6,8\text{-}C_2B_7H_{12}} + \underset{\mathbf{4}}{7\text{-}(C_5H_{11})\text{-}\textit{arachno}\text{-}6,8\text{-}C_2B_7H_{12}} \quad (3)$$

$$\textit{arachno}\text{-}6,8\text{-}C_2B_7H_{13} + \text{xs } H_2C{=}CH(C_6H_5) \xrightarrow{H_2PtCl_6{\cdot}6H_2O \text{ or } PtBr_2} \underset{\mathbf{5}}{7\text{-}(\textit{trans}\text{-}(C_6H_5)CH{=}CH)\text{-}\textit{arachno}\text{-}6,8\text{-}C_2B_7H_{12}} + \underset{\mathbf{6}}{7\text{-}((C_6H_5)CH_2CH_2)\text{-}\textit{arachno}\text{-}6,8\text{-}C_2B_7H_{12}} \quad (4)$$

GC/MS and ^{11}B NMR spectroscopic analyses of the $H_2PtCl_6{\cdot}6H_2O$ (3 mol %, 20 h) and $PtBr_2$ (10 mol %, 90 h) catalyzed 1-pentene reactions showed 88% and 89% conversions to the two major products **3** and **4**, corresponding to 27 and 9 catalyst turnovers, respectively. The $H_2PtCl_6{\cdot}6H_2O$ (7 mol %, 35 h) and $PtBr_2$ (10 mol %, 24 h) catalyzed styrene reactions afforded 74% and 86% conversions to a mixture of **5** and **6**, which corresponds to 12 and 8 catalyst turnovers, respectively. Minor amounts of higher substituted alkyl- and alkenyl-substituted derivatives along with some unreacted *arachno*-6,8-$C_2B_7H_{13}$ were also present in the reaction mixture.

The chloroplatinic acid-catalyzed reaction required elevated temperatures (60 °C), while the platinum(II) bromide catalyst was active at room temperature. Toluene was required as a solvent in the chloroplatinic acid-catalyzed reaction of styrene to prevent gelling of the reaction solution. Longer reaction times resulted in increased amounts of di- and trialkyl- and -alkenyl-substituted derivatives, but no change in the relative ratio of the 7-alkyl and 7-alkenyl products. Separation and purification of the products by flash column chromatography yielded analytically pure samples in the yields given in Table 1.

Palladium(II) Bromide-Catalyzed Reaction of 1-Pentene and Styrene with *arachno*-6,8-$C_2B_7H_{13}$. Whereas the $PdBr_2$-catalyzed reactions with ethylene afforded a mixture of hydroboration and dehydrogenative borylation products, the $PdBr_2$-catalyzed reaction of *arachno*-6,8-$C_2B_7H_{13}$ with 1-pentene (20 mol %, 6 h) or styrene (10 mol %, 18 h) resulted in exclusive conversion to the 7-(*trans*-R-CH=CH)-*arachno*-6,8-$C_2B_7H_{12}$ products **3** (84%) and **5** (85%) resulting from dehydrogenative borylation (eqs 5 and 6).

$$\textit{arachno}\text{-}6,8\text{-}C_2B_7H_{13} + \text{xs } H_2C{=}CH(CH_2)_2CH_3 \xrightarrow[32\ ^\circ C]{PdBr_2} \underset{\mathbf{3}}{7\text{-}(\textit{trans}\text{-}CH_3(CH_2)_2CH{=}CH)\text{-}\textit{arachno}\text{-}6,8\text{-}C_2B_7H_{12}} \quad (5)$$

$$\textit{arachno}\text{-}6,8\text{-}C_2B_7H_{13} + \text{xs } H_2C{=}CH(C_6H_5) \xrightarrow[32\ ^\circ C]{PdBr_2} \underset{\mathbf{5}}{7\text{-}(\textit{trans}\text{-}(C_6H_5)CH{=}CH)\text{-}\textit{arachno}\text{-}6,8\text{-}C_2B_7H_{12}} \quad (6)$$

Reactions run at room temperature showed no activity, while those at temperatures above ~40 °C gave no greater than 30%

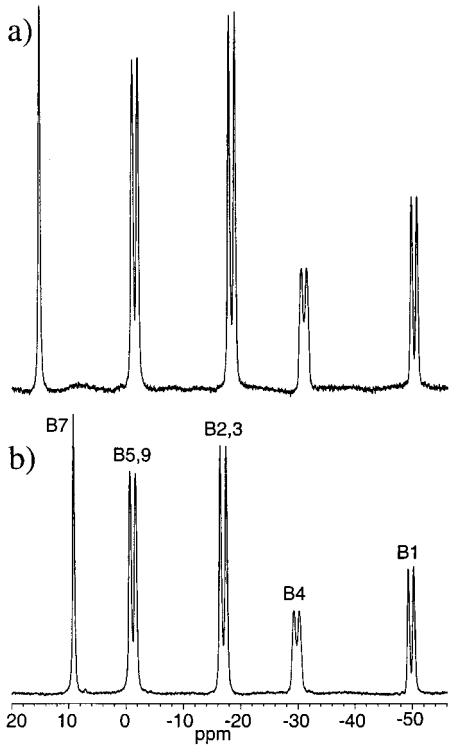

Figure 1. ^{11}B NMR (160.5 MHz) spectra of (a) 7-(C_2H_5)-*arachno*-6,8-$C_2B_7H_{12}$ (**1**) and (b) 7-(CH_2═CH)-*arachno*-6,8-$C_2B_7H_{12}$ (**2**).

conversion even when allowed to react for several days. ^{1}H NMR analysis of the volatile components of the styrene reaction revealed the formation of at least 1 equiv of ethylbenzene relative to the amount of 7-(*trans*-(C_6H_5)CH═CH)-*arachno*-6,8-$C_2B_7H_{12}$ (**5**) formed during the reaction. Purification and isolation of the products by flash column chromatography afforded moderate yields of analytically pure **3** and **5** (Table 1).

Spectroscopic, Crystallographic, and Computational Characterizations. *Spectroscopic Analysis***.** The NMR data for all compounds are given in Table 2. The ^{11}B NMR spectra for the 7-alkyl products **1** (Figure 1a), **4**, and **6** each showed a 1(s)/2(d)/2(d)/1(d)/1(d) pattern, indicating C_s symmetry, with the low-field singlet resonance consistent with substitution at that boron position. Jelínek and co-workers[19] have previously shown that nucleophilic attack of Bu^- ion on *arachno*-6,8-$C_2B_7H_{13}$ results in Bu substitution at the boron (B7) situated between the two carbon vertices of the dicarbaborane. The ^{11}B NMR chemical shifts for **1**, **4**, and **6** are nearly identical to those reported for 7-Bu-*arachno*-6,8-$C_2B_7H_{12}$ (14.94 (s), −1.95 (d), −19.00 (d), −31.66 (d), and −51.26 (d) ppm), thus supporting their 7-R-*arachno*-6,8-$C_2B_7H_{12}$ formulations.

The NMR assignments discussed above were confirmed using DFT/GIAO computations. These calculations use density functional theory (DFT) to obtain an optimized molecular geometry, followed by gauge-independent atomic orbital (GIAO) NMR shift calculations to predict the chemical shifts and assignments of each atom in the structure. Such computations have now been shown to be amazingly reliable in correctly predicting experimentally determined chemical shifts and assignments of polyborane clusters and have thus provided a powerful new tool for structure elucidation.[14,15,20] As shown in Table 2, the DFT/GIAO/NMR values calculated at the B3LYP/6-311G*//B3LYP/6-311G* level for **1** are, in fact, in excellent agreement with

(19) Jelínek, T.; Heřmánek, S.; Štíbr, B.; Plešek, J. *Polyhedron* **1986**, *5*, 1303.

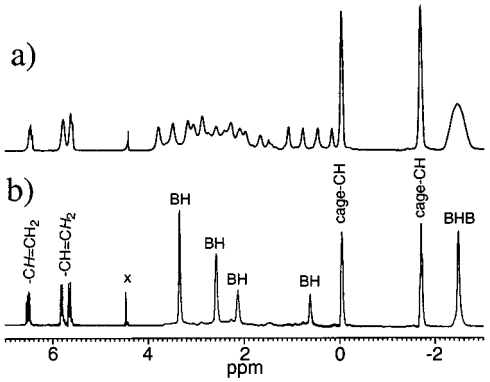

Figure 2. ^{1}H NMR (500.4 MHz) spectra of 7-(CH_2═CH)-*arachno*-6,8-$C_2B_7H_{12}$ (**2**): (a) ^{11}B-coupled and (b) ^{11}B-decoupled.

the experimentally determined ^{11}B chemical shifts and assignments (from 2D ^{11}B−^{11}B COSY experiments) for **1**, **4**, and **6**.

In addition to the proton resonances of their hydrocarbon substituents, the ^{11}B-decoupled ^{1}H NMR spectra for **1**, **4**, and **6** each show the two cage-CH resonances of the *endo*- and *exo*-hydrogens on the 6,8-CH_2 groups, a bridge hydrogen resonance of intensity 2 at high field, and resonances arising from the six terminal BH groups in the expected ratios of 2/2/1/1. The ^{13}C NMR spectrum of **1** shows a resonance at −11.57 ppm corresponding to the equivalent 6,8-cage carbons and the two ethyl carbon resonances at 10.45 and 12.65 ppm. The peak at 10.45 ppm shows a multiplet coupling pattern characteristic of $J_{^{13}C-^{11}B}$, leading to its assignment to the boron-bonded methylene carbon of the ethyl group. The observed $J_{^{13}C-^{11}B}$ of 72 Hz is consistent with the $J_{^{13}C-^{11}B}$ values that have been reported for alkylated carbaboranes.[20i,21]

The ^{11}B NMR spectra for the 7-alkenyl compounds **2** (Figure 1b), **3**, and **5** show a pattern similar to that found for **1**, **4**, and **6**, with the exception that the low-field singlet B7 resonance is shifted upfield in **2** (9.0 ppm), **3** (10.3 ppm), and **5** (9.6 ppm) relative to its shift in the alkyl derivatives **1** (15.3 ppm), **4** (14.8 ppm), and **6** (13.7 ppm). The DFT/GIAO calculations on **2** are again in excellent agreement with the experimentally determined values (Table 2), and correctly predict the upfield shift (calcd, $\Delta_\delta = -5.7$ ppm; exptl, $\Delta_\delta = -6.3$ ppm) of the B7 vertex in **2** relative to that found in **1**.

The ^{11}B-decoupled ^{1}H NMR spectra of **2** (Figure 2), **3**, and **5** are again similar to those observed for **1**, **4**, and **6** showing the two cage-CH_2 resonances, the upfield bridge hydrogen resonance, and the 2/2/1/1 pattern of the remaining terminal B−H vertexes. However, each compound also exhibits peaks between 5.9 and 6.9 ppm arising from the olefinic protons. The ^{13}C NMR spectra for both **2** and **3** contain the −11 ppm cage carbon resonance. The spectrum for **3** also clearly resolves each carbon of the alkenyl substituent, with two peaks in the olefinic region at 128.48 and 143.58 ppm and three peaks in the alkyl region at 37.75, 22.13, and 13.73 ppm. The peak at 128.48 ppm

(20) (a) Bühl, M.; Schleyer, P. v. R. *J. Am. Chem. Soc.* **1992**, *114*, 477. (b) Bühl, M.; Gauss, J.; Hofmann, M.; Schleyer, P. v. R. *J. Am. Chem. Soc.* **1993**, *115*, 12385. (c) Onak, T.; Tran, D.; Tseng, J.; Diaz, M.; Arias, J.; Herrera, S. *J. Am. Chem. Soc.* **1993**, *115*, 9210. (d) Diaz, M.; Jaballas, J.; Arias, J.; Lee, H.; Onak, T. *J. Am. Chem. Soc.* **1996**, *118*, 4405. (e) Bausch, J. W.; Matoka, D. J.; Carroll, P. J.; Sneddon, L. G. *J. Am. Chem. Soc.* **1996**, *118*, 11423. (f) Jaballas, J.; Onak, T. *J. Organomet. Chem.* **1998**, *550*, 101. (g) Cranson, S. J.; Fox, M. A.; Greatrex, R.; Greenwood, N. N. *J. Organomet. Chem.* **1998**, *550*, 207. (h) Hofmann, M.; Fox, M. A.; Greatrex, R.; Williams R. E.; Schleyer, P.v. R. *J. Organomet. Chem.* **1998**, *550*, 331. (i) Onak, T.; Jaballas, J.; Barfield, M. *J. Am. Chem. Soc.* **1999**, *121*, 2850. (j) Shedlow, A. M.; Sneddon, L. G. *Inorg. Chem.* **1998**, *37*, 5269.

(21) Wrackmeyer, B. *Prog. NMR Spectrosc.* **1979**, *12*, 227.

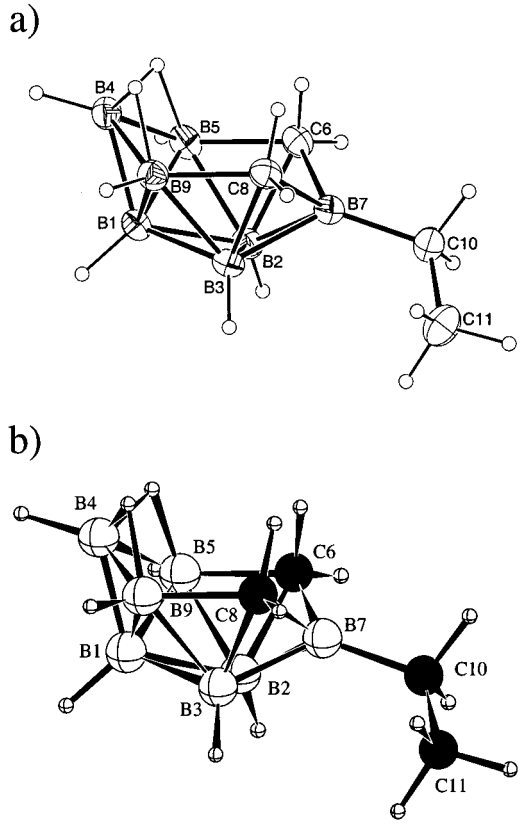

Figure 3. (a) X-ray crystallographic and (b) DFT (B3LYP/6-311G* level) optimized structures for 7-(C_2H_5)-*arachno*-6,8-$C_2B_7H_{12}$ (**1**).

also shows a $J_{^{13}C-^{11}B}$ of 108 Hz which is 36 Hz greater than that observed for the alkyl derivative **1**, indicating, as expected, a higher degree of s-character in the B7−C10 bond of the alkenyl derivative **3** relative to **1**.[21]

The IR spectra of **1**, **2**, **3**, **4**, **5,** and **6** all show characteristic B−H and C−H absorptions in the 2560−2590 and 2910−3060 cm^{-1} regions. The spectra of **2**, **3**, and **5** also contain a peak between 1600 and 1620 cm^{-1} corresponding to the olefinic double-bond stretch.

Crystallographic and Computational Analysis. Elucidation of the detailed structure of the alkyl-substituted 7-(C_2H_5)-*arachno*-6,8-$C_2B_7H_{12}$ (**1**) was obtained by both X-ray crystallographic and DFT computational studies. The crystallographically determined structure of **1** is shown in the ORTEP diagram in Figure 3a, while its DFT-optimized geometry at the B3LYP/6-311G* level is depicted in Figure 3b. These structural studies confirm both the C_s symmetry indicated by the NMR studies and that hydroboration has occurred at the B7 vertex of the *arachno*-6,8-$C_2B_7H_{13}$ carbaborane.

There is excellent agreement between the trends observed in the crystallographic and DFT-calculated values for the distances and angles in **1** (Table 4). These values are also in the ranges found in the crystallographically determined structure of *arachno*-6,8-$Me_2C_2B_7H_{11}$,[22] as well as the crystallographically determined[23] and DFT-calculated structures (Figure 4) of *arachno*-6,8-$C_2B_7H_{13}$ (**7**). As diagrammed in Figure 7, the only significant difference between the structure of the parent compound *arachno*-6,8-$C_2B_7H_{13}$ (**7**) and 7-(C_2H_5)-*arachno*-6,8-$C_2B_7H_{12}$ (**1**) is that, in **1**, the C6−B7 and C8−B7 lengths are longer (∼0.03−0.04 Å) than in **7**, perhaps reflecting an increased bonding interaction of B7 with the alkyl carbon in **1** relative to its hydrogen substituent in **7**.

(22) Voet, D.; Lipscomb, W. N. *Inorg. Chem.* **1967**, *6*, 113.
(23) Kang, S. O.; Sneddon, L. G. Unpublished results.

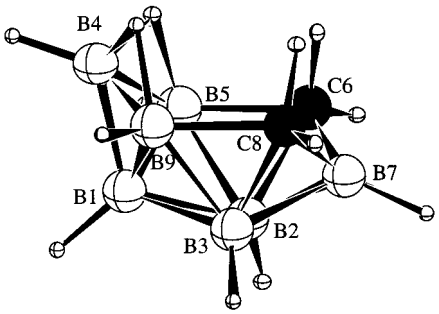

Figure 4. DFT (B3LYP/6-311G* level) optimized geometry for *arachno*-6,8-$C_2B_7H_{13}$ (**7**). Selected bond distances (Å) and angles (deg): B(7)−C(6) 1.705, B(7)−C(8) 1.704, B(2)−B(7) 1.741, B(3)−B(7) 1.742, B(5)−C(6) 1.716, B(9)−C(8) 1.716; C(6)−B(7)−C(8) 108.3, B(5)−C(6)−B(7) 113.1, B(9)−C(8)−B(7) 113.0.

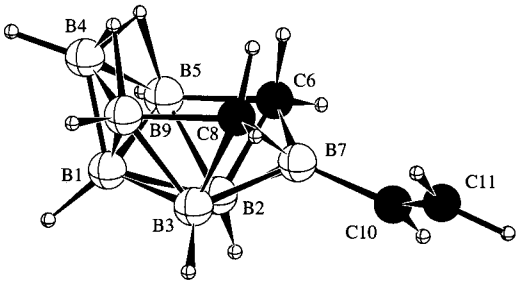

Figure 5. DFT (B3LYP/6-311G* level) optimized geometry for 7-(CH_2═CH)-*arachno*-6,8-$C_2B_7H_{12}$ (**2**).

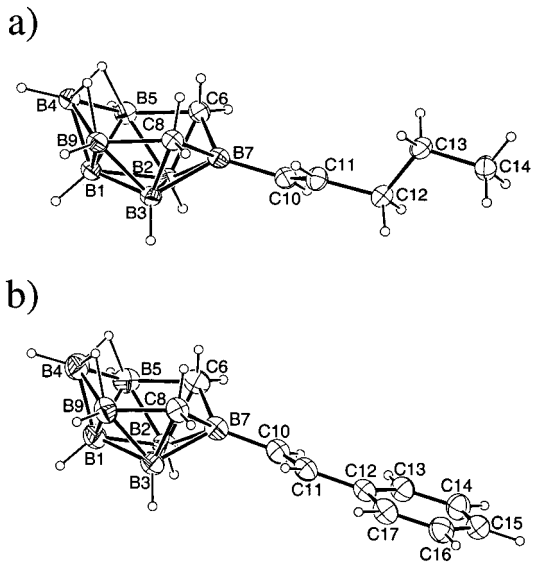

Figure 6. X-ray crystallographic structures of (a) 7-(*trans*-$CH_3(CH_2)_2$-CH═CH)-*arachno*-6,8-$C_2B_7H_{12}$ (**3**) and (b) 7-(*trans*-(C_6H_5)-CH═CH)-*arachno*-6,8-$C_2B_7H_{12}$ (**5**).

The DFT-optimized geometry for 7-(CH_2═CH)-*arachno*-6,8-$C_2B_7H_{12}$ (**2**) is presented in Figure 5, and the X-ray crystallographically determined structures of 7-(*trans*-$CH_3(CH_2)_2CH$═CH)-*arachno*-6,8-$C_2B_7H_{12}$ (**3**) and 7-(*trans*-(C_6H_5)CH═CH)-*arachno*-6,8-$C_2B_7H_{12}$ (**5**) are shown in the ORTEP drawings in Figure 6. These structural studies establish that, in **2**, **3,** and **5**, substitution has again occurred at the B7 position but, more importantly, confirm that these compounds, unlike **1**, **4,** and **6**, have alkenyl substituents that have been produced by dehydrogenative borylation of the olefins at the terminal olefinic carbon. The C10−C11 double-bond lengths observed in **3** (1.322(2) Å)

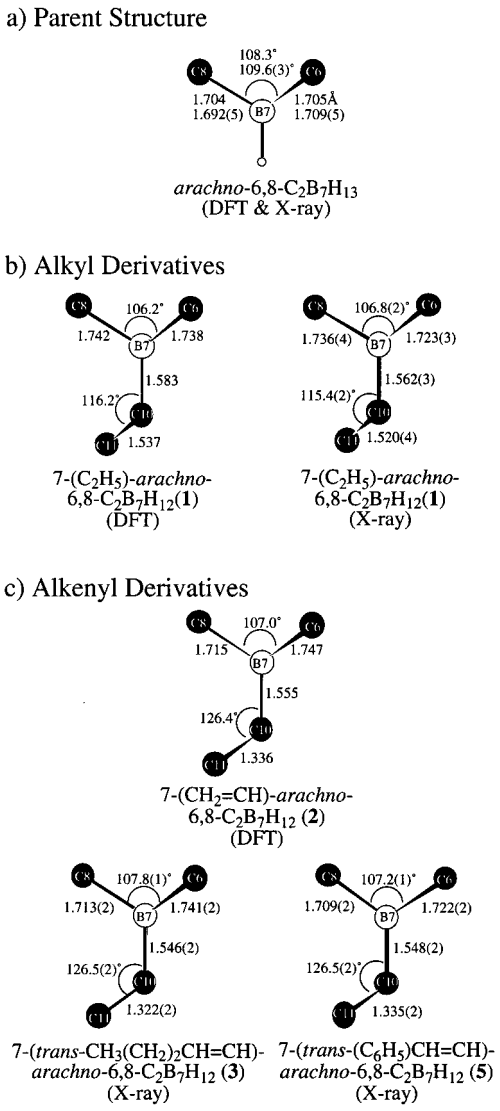

Figure 7. (a) DFT and X-ray (with errors) bond lengths and angles for *arachno*-6,8-$C_2B_7H_{13}$ (**7**). (b) DFT and X-ray bond lengths and angles for 7-(C_2H_5)-*arachno*-6,8-$C_2B_7H_{12}$ (**1**) [dihedral angles (C8−B7−C10−C11) (DFT) 53.4°, (X-ray) 57.7°]. (c) DFT and X-ray bond lengths and angles for 7-(CH_2═CH)-*arachno*-6,8-$C_2B_7H_{12}$ (**2**; DFT), 7-(*trans*-$CH_3(CH_2)_2$CH═CH)-*arachno*-6,8-$C_2B_7H_{12}$ (**3**; X-ray), and 7-(*trans*-(C_6H_5)CH═CH)-*arachno*-6,8-$C_2B_7H_{12}$ (**5**; X-ray) [dihedral angles (C8−B7−C10−C11) (**2**) −5.9°, (**3**) −6.6°, (**5**) 11.9°].

and **5** (1.335(2) Å) are in excellent agreement with that calculated for **2** (1.336 Å).

As noted above, the C6−B7 and C8−B7 distances in **1**, **4,** and **6** are somewhat longer than those found in the parent carbaborane **7**, but within experimental error, they are equivalent. However, in the alkenyl-substituted compounds **2**, **3,** and **5** there is a pronounced asymmetry. Thus, as diagrammed in Figure 7, in both the DFT-optimized geometry of **2** and the crystallographically determined structures of **3** and **5**, the C8−B7 bond lengths are substantially shorter (1.715 Å, **2**; 1.713(2) Å, **3**; 1.709(2) Å, **5**) than the C6−B7 bond lengths (1.747 Å, **2**; 1.741(2) Å, **3**; 1.722(2) Å, **5**). Along with the shortening of the C8−B7 bond, the C8−B9 bond in **2**, **3,** and **5** is lengthened (1.711 Å, **2**; 1.689 Å, **3**; 1.695 Å, **5**) relative to the B5−C6 bond (1.691 Å, **2**; 1.669 Å, **3**; 1.679 Å, **5**). Additionally, in **2**, **3,** and **5** the C8−B7−C10−C11 atoms are all nearly coplanar and the C10−C11 double bond is oriented in a *cisoid* fashion relative to the C8−B7 bond. The crystallographically determined dihedral angles (C8−B7−C10−C11 axis) for **3** (−6.6(3)°) and **5** (11.9(2)°) compare well with the calculated dihedral angle for **2** (−5.9°). This planarity contrasts with the structure of **1**, where the dihedral angle about the C8−B7−C10−C11 axis was crystallographically determined to be 57.7(1)° (calculated 53.6°).

The crystallographic B7−C10 bond lengths in the 7-alkenyl-substituted derivatives **3** (1.546(2) Å) and **5** (1.548(2) Å) are also shorter than that of the 7-alkyl-substituted derivative **1** (1.562(3) Å). Likewise, the DFT-optimized B7−C10 bond lengths for **2** (1.555 Å) and **1** (1.583 Å) show the same trend. The shorter B7−C10 bond lengths for the alkenyl derivatives are also consistent with the larger $J_{13_C-11_B}$ couplings, discussed above, between these atoms in the NMR spectra of **3** relative to **1**. These trends in the B7−C10 bond lengths and coupling constants and, in particular, the greatly shortened cage C8−B7 bond and *cisoid* planar orientation of the C8−B7 and C10−C11 atoms strongly suggest that there is a π-bonding interaction between the olefin and the B7 boron. This could involve donation of π-electron density from the olefin into an orbital on the B7 atom that is oriented perpendicular to the C8−B7−C10−C11 plane. This increased electron density on B7 would then enhance greater π-bonding interactions between the B7 and C8 cage atoms, thus increasing the C8−B7 bond order and decreasing the C8−B7 distance. Indeed, both the *cisoid* planar orientation of the C8−B7−C10−C11 atoms and the trends observed in their bond lengths are reminiscent of the features that appear in organic conjugated diolefins.[24]

Discussion

Studies of the detailed mechanisms of the platinum- and palladium-catalyzed reactions were not undertaken; however, the observed reactivities and product distributions in the reactions of these catalysts with *arachno*-6,8-$C_2B_7H_{13}$ are consistent with previous results for their use in metal-catalyzed olefin hydrosilations, as well as other polyborane olefin hydroborations. Thus, several general conclusions and reasonable mechanistic pathways can be proposed.

A possible reaction sequence for the platinum-catalyzed reactions of olefins with *arachno*-6,8-$C_2B_7H_{13}$ is illustrated in Figure 8. For those reactions employing chloroplatinic acid, an induction period of several hours was observed during which time the reaction solution underwent a slow change from a clear solution with undissolved solid catalyst to a brown-black solution with a suspended black solid. This induction period is entirely consistent with the known chloroplatinic acid-catalyzed olefin hydrosilations[25] and decaborane olefin hydroborations,[2] where the initial reduction of Pt(IV) to a catalytically active Pt(II) species has been proposed. The platinum(II) bromide-catalyzed reactions proceeded without any observable induction period, again suggesting that Pt(II) is the active catalytic species. We also found that sources of Pt(0) species, such as Karstedt's catalyst,[26] were inactive, providing evidence that the Pt(II)/Pt(IV) cycle is the active catalyst system in the *arachno*-6,8-$C_2B_7H_{13}$ reactions. Thus, as diagrammed in the figure, following olefin association, oxidative addition[27] of the *arachno*-6,8-$C_2B_7H_{13}$ carbaborane to the Pt(II) center would result in the formation of the Pt(IV) product **A**. The high product selectivity

(24) Benet-Buchholz, J.; Boese, R.; Haumann, T.; Traetteberg, M. In *The Chemistry of Dienes and Polyenes*; Rappoport, Z., Ed.; Wiley: Chichester, 1997; p 25.

(25) Speier, J. L. *Adv. Organomet. Chem.* **1979**, *17*, 407.

(26) Lewis, L. N.; Lewis, N.; Uriarte, R. J. In *Homogeneous Transition Metal Catalyzed Reactions*; Moser, W. R., Slocum, D. W., Eds.; Advances in Chemistry Series 230; American Chemical Society: Washington, DC, 1992; p 541.

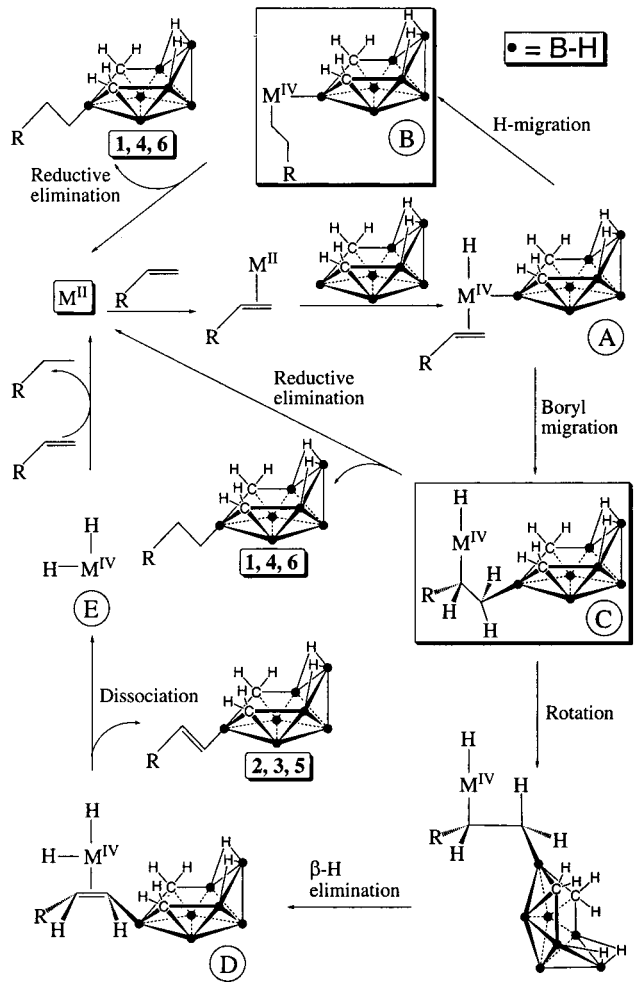

Figure 8. Possible reaction mechanism for the formation of both hydroboration and dehydrogenative borylation products.

observed for functionalization at the B7 position indicates that oxidative addition occurs exclusively at this vertex. Owing to its location between the two carbon cage atoms, B7 is, in fact, the most positive vertex in the *arachno*-6,8-$C_2B_7H_{13}$ cage,[28] and catalyst attack at this position is consistent with the previously observed reactivity patterns found in the platinum(II)-catalyzed reactions of olefins and decaborane(14).[2] Hydride migration to the olefin in complex **A** to produce **B**, followed by reductive elimination, provides a straightforward pathway to the 7-alkyl products **1**, **4,** and **6**. Alternatively, boryl migration to the olefin in complex **A** could occur to produce complex **C**. If **C** then undergoes reductive elimination, 7-alkyl products are again produced. However, if instead of reductive elimination, β-hydride elimination occurs to produce **D**, followed by dissociation of the substituted olefin, then the 7-alkenyl products **2**, **3,** and **5** would result. Such dehydrogenative borylation[29] and the related dehydrogenative silylation[30] reactions are well-known and have been proposed to occur by such mechanisms. The alkyl/alkenyl product ratio is then controlled by the relative hydride versus boryl (or silyl) migration and/or β-hydride elimination versus reductive elimination rates. Previous studies of related metal-catalyzed hydrosilations and hydroborations have shown that these rates strongly depend on the reaction conditions and the particular metal, olefin, and substrates.[25,31]

All products resulted from either addition or substitution of the borane at the terminal olefinic carbon, with the dehydrogenative borylation products also exhibiting exclusively *trans*-stereochemistry. The platinum-catalyzed reaction of ethylene affords exclusively the hydroboration product **1**, whereas the platinum-catalyzed reactions of 1-pentene and styrene yield mixtures of hydroboration and dehydrogenative borylation products. These observations are consistent with the previous studies of transition-metal-catalyzed hydrosilations[30] and catechol borane hydroborations,[29] where, in both cases, it was found that sterically bulky olefins favor dehydrogenative substitution relative to addition. This difference is proposed to result from the greater repulsive interactions of bulkier metalloalkyls with the metal center, borane or silane, and other coordinated ligands. These repulsions then increase the rate of β-hydride elimination relative to reductive elimination. The fact that both the platinum and palladium reactions with 1-pentene and styrene afford the 7-*trans*-alkenyl products is also likely determined by the steric interactions in complex **C** (Figure 8) between the metal center and the borylalkyl. Thus, rotation about the carbon−carbon bond of the borylalkyl complex to minimize steric interactions with the boryl group would place a β-hydrogen in close proximity to the metal center, thus facilitating β-H elimination with retention of the *trans*-conformation.[29]

While platinum-catalyzed dehydrogenative borylation has apparently not been observed before, we have already shown that these types of reactions are favored for the palladium(II)-catalyzed reactions of other polyboranes, such as pentaborane-(9)[3,4] and borazine.[5] These prior results, plus the observation that the palladium(II) bromide-catalyzed reactions of olefins with *arachno*-6,8-$C_2B_7H_{13}$ yield predominantly alkenyl products, suggest that the boryl migration/β-hydride elimination pathway is more favorable for Pd(II) than Pt(II) metal centers.

The optimum temperature for the palladium-catalyzed reactions was found to be 32 °C. Reactions at room temperature were very slow, while those run at higher than 40 °C appeared

(27) The mechanism presented in Figure 8 assumes that B−H oxidative addition of *arachno*-6,8-$C_2B_7H_{13}$ is a key step. However, others have proposed that, in metal-catalyzed hydosilations and hydroborations, the reaction of the metalloolefin with the silane or borane substrate occurs instead by a σ-bond metathesis mechanism involving the direct addition of a Si−H or B−H bond across the M−C bond of the coordinated olefin. Thus, an alternate mechanism is also possible for the *arachno*-6,8-$C_2B_7H_{13}$ reactions reported herein. See, for example: Hartwig, J. F.; Bhandari, S.; Rablen, P. R. *J. Am. Chem. Soc.* **1994**, *116*, 1839.

(28) Dolansky, J.; Hermánek, S.; Zahradník *Collect. Czech. Chem. Commun.* **1981**, *46*, 2479.

(29) (a) Männig, D.; Nöth, H. *Angew. Chem., Int. Ed. Engl.* **1985**, *24*, 878. (b) Evans, D. A.; Fu, G. C.; Anderson, B. A. *J. Am. Chem. Soc.* **1992**, *114*, 6679. (c) Burgess, K.; van der Donk, W. A.; Westcott, S. A.; Marder, T. B.; Baker, R. T.; Calabrese, J. C. *J. Am. Chem. Soc.* **1992**, *114*, 9350. (d) Baker, R. T.; Calabrese, J. C.; Westcott, S. A.; Nguyen, P.; Marder, T. B. *J. Am. Chem. Soc.* **1993**, *115*, 4367. (e) Westcott, S. A.; Marder, T. B.; Baker, R. T. *Organometallics* **1993**, *12*, 975. (f) Brown, J. M.; Lloyd-Jones, G. C. *J. Am. Chem. Soc.* **1994**, *116*, 866. (g) Musaev, D. G.; Mebel, A. M.; Morokuma, K. *J. Am. Chem. Soc.* **1994**, *116*, 10693. (h) Baker, R. T.; Calabrese, J. C.; Westcott, S. A.; Marder, T. B. *J. Am. Chem. Soc.* **1995**, *117*, 8777. (i) Dorigo, A. E.; Schleyer, P.v. R. *Angew. Chem., Int. Ed. Engl.* **1995**, *34*, 115. (j) Marder, T. B.; Norman, N. C. *Top. Catal.* **1998**, *5*, 63. (k) Murata, M.; Watanabe, S.; Masuda, Y. *Tetrahedron Lett.* **1999**, *40*, 2585. (l) Vogels, C. M.; Hayes, P. G.; Shaver, M. P.; Westcott, S. A. *Chem. Commun.* **2000**, 51. (m) Widauer, C.; Grützmacher, H.; Ziegler, T. *Organometallics* **2000**, *19*, 2097.

(30) (a) Onopchenko, A.; Sabourin, E. T.; Beach, D. L. *J. Org. Chem.* **1983**, *48*, 5101. (b) Ojima, I.; Fuchikami, T.; Yatabe, M. *J. Organomet. Chem.* **1984**, *260*, 335. (c) Onopchenko, A.; Sabourin, E. T.; Beach, D. L. *J. Org. Chem.* **1984**, *49*, 3389. (d) Randolph, C. L.; Wrighton, M. S. *J. Am. Chem. Soc.* **1986**, *108*, 3366. (e) Ojima, I. In *The Chemistry of Organic Silicon Compounds*; Patai, S., Rappoport, Z., Eds.; Wiley: New York, 1989; pp 1479−1526. (f) Tanke, R. S.; Crabtree, R. H. *Organometallics* **1991**, *10*, 415. (g) Brookhart, M.; Grant, B. E. *J. Am. Chem. Soc.* **1993**, *115*, 2151. (h) Christ, M. L.; Sabo-Etienne, S.; Chaudret, B. *Organometallics* **1995**, *14*, 1082. (i) Takeuchi, R.; Yasue, H. *Organometallics* **1996**, *15*, 2098. (j) LaPointe, A. M.; Rix, F. C.; Brookhart, M. *J. Am. Chem. Soc.* **1997**, *119*, 906. (k) Marciniec, B. *New J. Chem.* **1997**, *21*, 815.

(31) Beletskaya, I.; Pelter, A. *Tetrahedron* **1997**, *53*, 4957.

to stop after only low conversions (~30%), suggesting catalyst deactivation. The **2**/**1** product ratios in the palladium-catalyzed reactions with ethylene were found to depend on the ethylene concentration. Thus, a reaction employing a 6-fold excess of ethylene gave a 3/1 preference for the dehydrogenative borylation product **2** over the hydroboration product **1**, while a ~13-fold excess of ethylene resulted in a 10/1 preference for **2** over **1**. These results are consistent with the fact that to have catalytic dehydrogenative borylation, an additional equivalent of olefin, either ethylene or **2**, is required to react with the dihydrido complex **E** in Figure 8 to regenerate the catalytically active Pd(II) species. Increasing the ethylene concentration would increase the rate of reaction of complex **E** with ethylene relative to **2,** thus enhancing the rate of the dehydrogenative-borylation reaction pathway. Since the 1-pentene and styrene reactions were run in neat olefin, the concentration of olefin was high and only dehydrogenative borylation products were observed. NMR studies of the reactions with styrene in fact confirmed that ethylbenzene and **5** were produced in equivalent amounts in these reactions.

In summary, both platinum and palladium species have been found to be active catalysts for the reactions of the *arachno*-6,8-$C_2B_7H_{13}$ dicarbaborane with olefins, and yield, depending upon the reaction conditions, catalyst, and/or olefin, alkyl- or alkenyldicarbaboranes resulting from either hydroboration or dehydrogenative borylation reactions, respectively. The key reaction steps for the dicarbaborane reactions appear to be closely related to those recently proposed for both metal-catalyzed olefin-hydrosilation/dehydrogenative-silylation and monoborane-hydroboration/dehydrogenative-borylation reactions. These results suggest that such catalysts may find applications for the generation of a variety of important alkyl- and alkenylpolyborane derivatives, and investigations to explore the scope of these catalysts are currently in progress.

Acknowledgment. We thank the National Science Foundation for support of this research.

Supporting Information Available: Tables listing refined positional and thermal parameters, bond distances and bond angles for compounds **1**, **3**, and **5** and Cartesian coordinates and bond distances for the optimized geometries at the B3LYP/6-311G* level for **1**, **2**, and **7** (PDF). This material is available free of charge via the Internet at http://pubs.acs.org.

JA002178R